Supplementary Information

Enhanced dielectric losses in α-MnO_2 via protonated modulation

Tengchao Guo,[ac] Yuejun Feng,[b] Bin Quan,[c] Yuhang Zhuang,*[d] Guomin Sun,[c] Liang Xue,[d] Lingzhe Fang*[e] and Xiaohui Zhu*[abc]

[a] Jiangsu Key Laboratory of Atmospheric Environment Monitoring and Pollution Control, Collaborative Innovation Center of Atmospheric Environment and Equipment Technology, School of Environmental Science and Engineering, Nanjing University of Information Science and Technology, Nanjing 210044, China

[b] Jiangyin Electrical Alloy Co., Ltd., Jiangyin 214423, China

[c] School of Chemistry and Materials Science, Nanjing University of Information Science and Technology, Nanjing 210044, China

[d] School of Materials Science and Engineering, Nanjing University of Science and Technology, Nanjing 210094, China

[e] Department of Chemistry and Biochemistry, Northern Illinois University, DeKalb, Illinois 60115, United States

E-mail: zhuangyuhang1995@163.com (Y. Zhuang), lfang@niu.edu (L. Fang), zhuxiaohui@nuist.edu.cn (X. Zhu)

Experimental section

Synthesis. The α-MnO_2 (M1) sample was prepared by a simple hydrothermal route. In detail, 3.5 g of $NaMnO_4$ solution (40 *wt*%, Aldrich) was mixed in 40 mL of deionized distilled water (18.2 MΩ cm resistivity). Then, 0.65 g of $MnSO_4 \cdot H_2O$ (99%, Aldrich) was added slowly into above mixed solution, transferred into a 50 mL Teflon-lined stainless steel autoclave, and heated at 180°C for 10 h. The as-prepared product was cleaned and filtered by deionized distilled water, and subsequently annealed at 80°C under a vacuum oven for 10 h, to obtain the M1 sample. For the protonated MnO_2 samples, 0.5 g of α-MnO_2 samples were immersed into 40 mL of H_2SO_4 solutions with *pH* values of 3, transferred into 50 mL Teflon-lined stainless steel autoclaves and heated at 100°C for 1 and 1.5 h, respectively. The as-obtained products were cleaned and filtered with deionized distilled water, and finally dried at 80°C under a vacuum oven for 10 h, to obtain the M2 and M3 samples, respectively.

Materials characterization. The chemical compositions of the M1–M3 samples were determined by inductively coupled plasma (ICP; Optima 4300DV) measurements. For the ICP test, the qualities of Mn or Na/Mn and total qualities of the samples were both obtained, and subsequently the final chemical formulas of the samples were calculated. The M1–M3 samples were mixed with KBr and pressed into pellets for further Fourier-transform infrared spectroscopy (FTIR; EQUINOX55) measurements. The thermogravimetric analysis (TGA; SDTA851E) was carried out at a heating rate of 5°C min^{-1} under N_2 flow. The crystallographic structures of the M1–M3 samples were investigated by synchrotron X-ray diffraction (SXRD; Argonne National Laboratory), and their corresponding SXRD patterns were further analyzed by the Rietveld refinement using General Structure Analysis System (GSAS) software. The surface morphologies and microstructures of the M1–M3 samples were characterized by field-emission scanning electron microscopy (FESEM; Hitachi S4300) and scanning transmission electron microscopy (STEM; TECNAI, Titan). The local structures of the M1–M3 samples were investigated by synchrotron sXAS measurements (Argonne National Laboratory).

EWA measurements. Electromagnetic parameters of the M1–M3 samples were measured by a vector network analyzer (PNAN5244A, Agilent) with same mass ratios between powder absorbers and paraffin of 7:3. The reflection loss (RL) values were obtained according to equations 1 and 2 as follows:[1,2]

$$RL = 20lg\left|\frac{Z_{in} - Z_0}{Z_{in} + Z_0}\right| \#(1)$$

$$Z_{in} = Z_0\sqrt{\frac{\mu_r}{\varepsilon_r}}tanh\left(j\frac{2\pi f d\sqrt{\mu_r\varepsilon_r}}{c}\right) \#(2)$$

where Z_{in}, Z_0, c, f, ε_r, μ_r, and d represent the normalized input impedance of the absorber, impedance of air, velocity of light, and frequency of microwaves, relative complex permittivity, relative complex permeability, and thickness of the absorber, respectively.

The electromagnetic parameters were investigated by the equations 3–6, respectively.[3,4] The σ, ω, ε_s, ε_∞, ε', ε'', ε''_c, ε''_p, and tanδ_ε parameters represent the leakage conductivity, angular frequency, static permittivity, relative dielectric permittivity at high frequency limit, real part of complex permittivity, imaginary part of complex permittivity, contribution of charge transport to ε'', contribution of relaxation to ε'', and dielectric loss tangent, respectively. The impedance matching value (Z) was investigated by the equation 7.[4]

$$\varepsilon_r = \varepsilon' - j\varepsilon'' \#(3)$$

$$\varepsilon''_c = \frac{\sigma}{\omega\varepsilon_0} \#(4)$$

$$\varepsilon''_p = \frac{\varepsilon_s - \varepsilon_\infty}{\omega\varepsilon_0} = \varepsilon'' - \varepsilon''_c \#(5)$$

$$tan\delta_\varepsilon = \frac{\varepsilon''}{\varepsilon'} \#(6)$$

$$Z = \left|\frac{Z_{in}}{Z_0}\right| \#(7)$$

Supplementary Figures

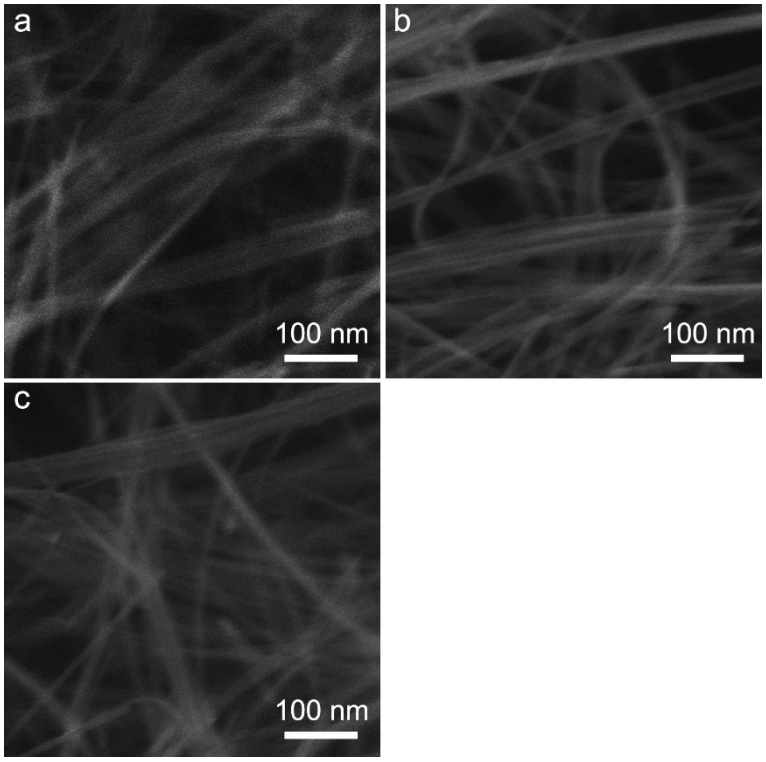

Fig. S1 Surface morphology. The FESEM images of the (a) M1, (b) M2, and (c) M3 samples, respectively.

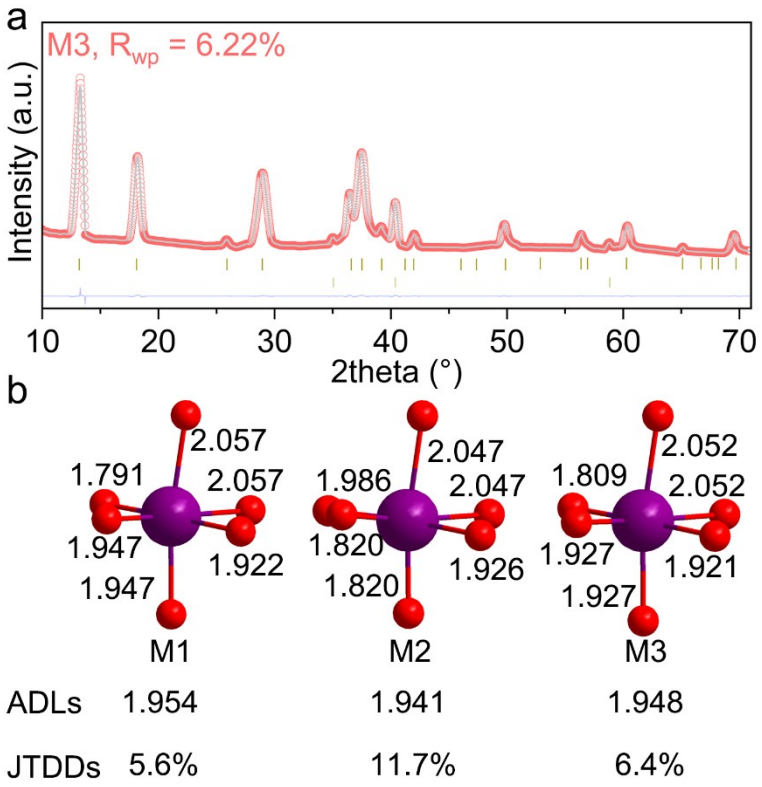

Fig. S2 Phase information. (a) Rietveld-refined SXRD patterns for the M3 sample. (b) Average bond lengths (ADLs) and Jahn–Teller distortion degrees (JTDDs) of MnO_6 octahedra in M1–M3. Average bond length was the average value of all bond lengths in MnO_6 octahedron.

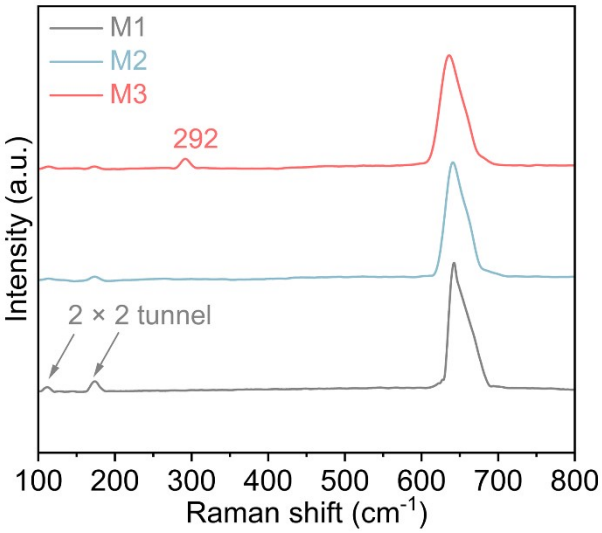

Fig. S3 Raman spectra. The Raman spectra of the M1–M3 samples.

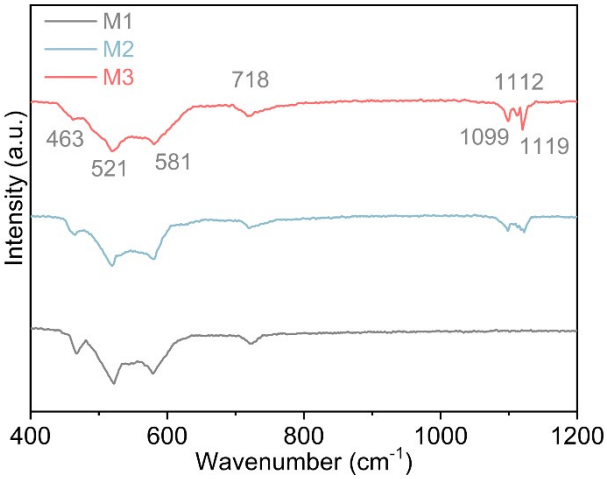

Fig. S4 FTIR spectra. The FTIR spectra of the M1–M3 samples.

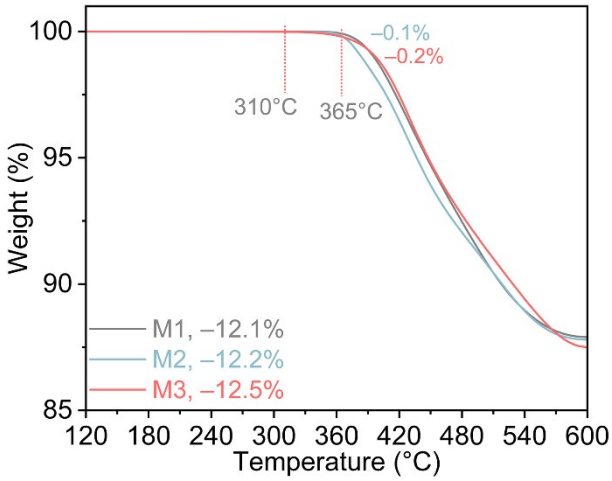

Fig. S5 TGA analysis. TGA curves of the M1–M3 samples.

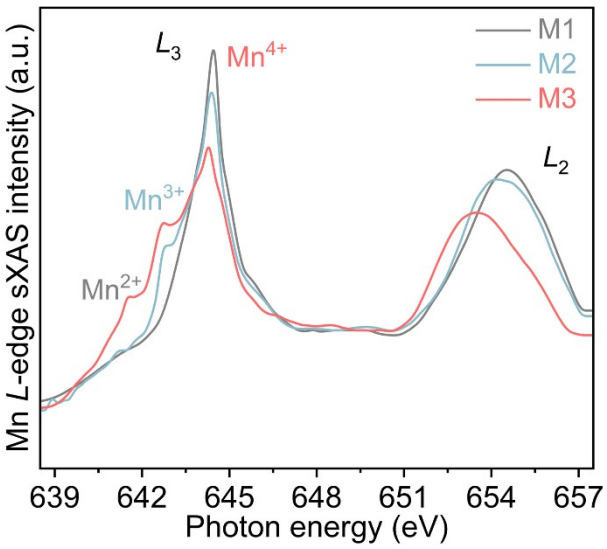

Fig. S6 sXAS spectra. Mn *L*-edge sXAS spectra of the M1–M3 samples in the FY mode.

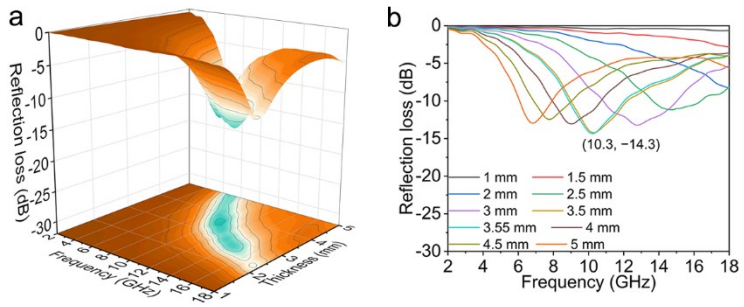

Fig. S7 EWA performance. The (a) 3D mappings and (b) line plots for RL–frequency curves of the M3 sample at the thicknesses of 1–5 mm in the frequency range of 2–18 GHz, respectively.

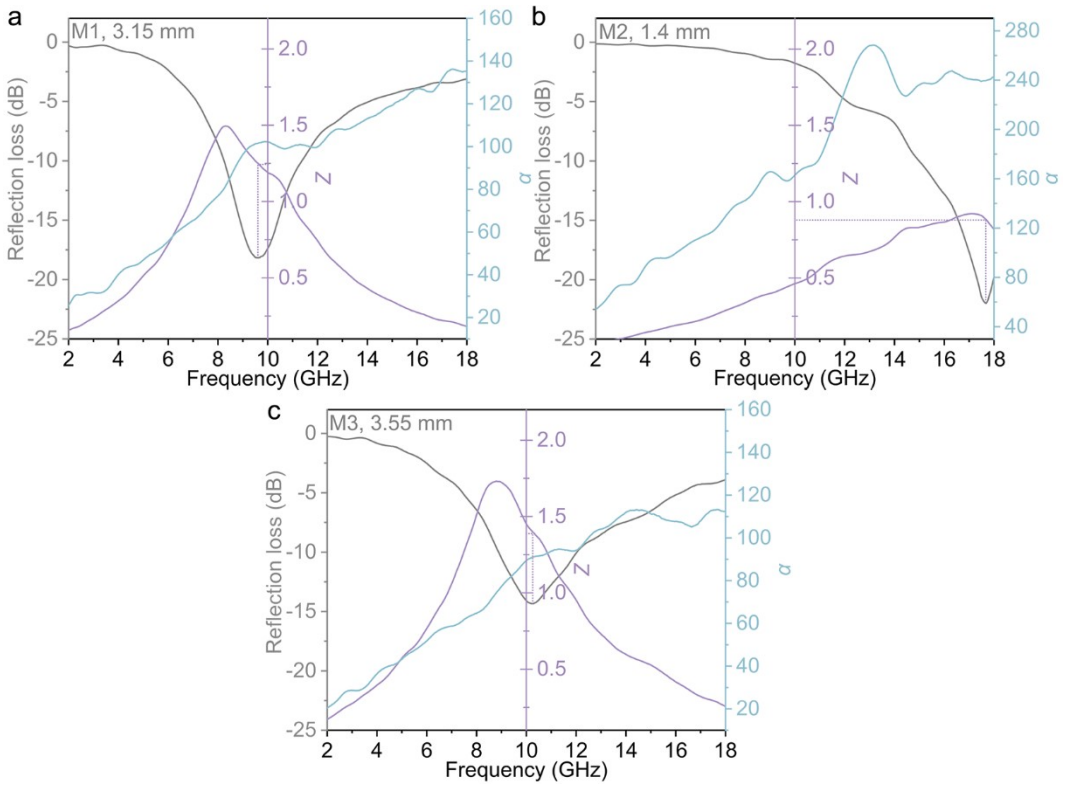

Fig. S8 EWA performance. The RL, *Z*, and *α*–frequency curves of the (a) M1, (b) M2, and (c) M3, respectively.

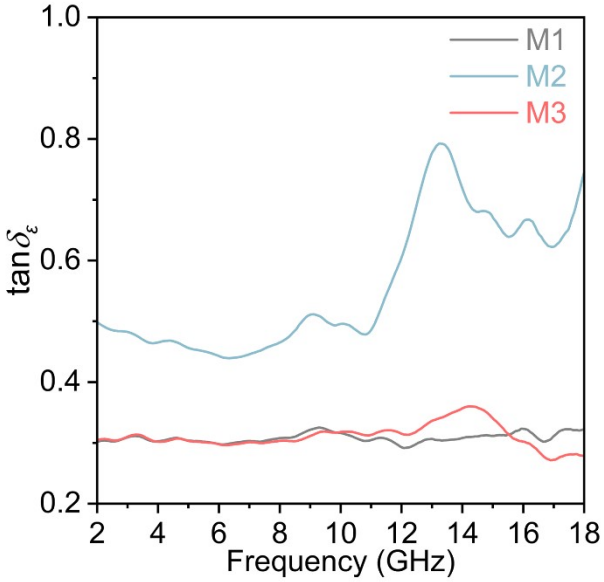

Fig. S9 Electromagnetic parameter. The tanδ_ε–frequency curves of the M1–M3 samples.

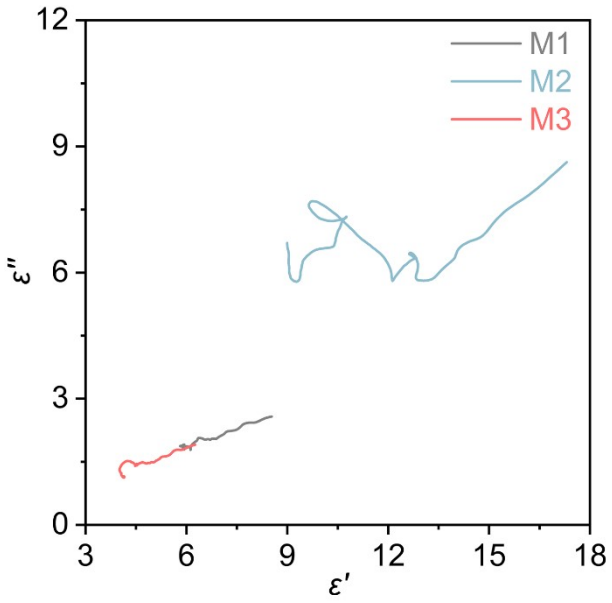

Fig. S10 Cole–Cole curves. The ε'–ε'' plots of the M1–M3 samples.

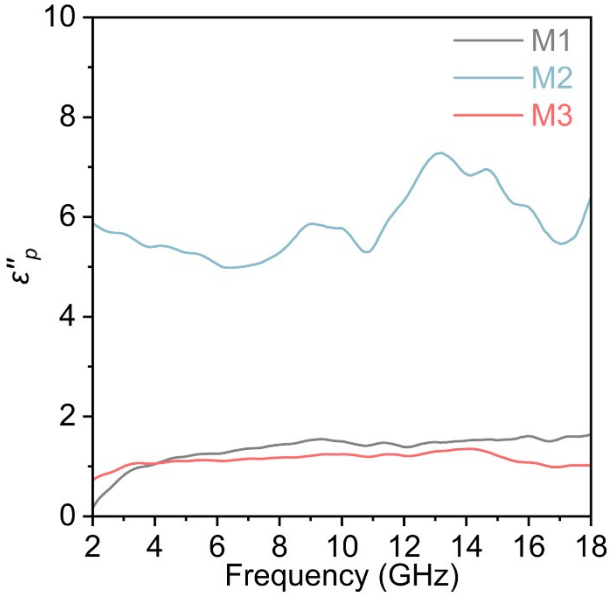

Fig. S11 Electromagnetic parameter. The ε''_p–frequency curves of the M1–M3 samples.

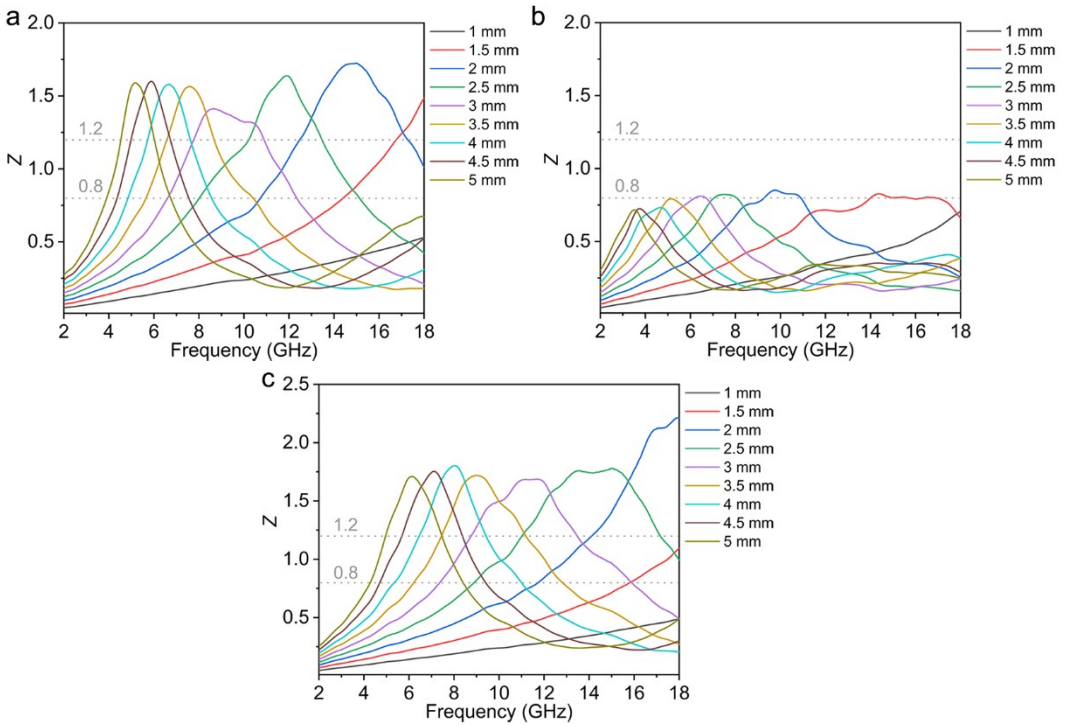

Fig. S12 Impedance matching. The impedance matching curves of the (a) M1, (b) M2, (c) M3 samples, respectively.

Supplementary Tables

Table S1. The obtained chemical compositions of M1–M3 by ICP analysis.

Sample	Chemical formula
M1	$Na_{0.05}MnO_2$
M2	$H_{0.08}MnO_2$
M3	$H_{0.15}MnO_2$

Table S2 Rietveld refinement parameters of the M1 sample from Fig. 1b.

Atom	***x***	***y***	***z***	**Occupancy**	***a*(Å)**	***c*(Å)**
Na	0	0	0.5	0.05		
Mn	0.3554	0.1718	0	1	9.798	2.859
O	0.1593	0.178	0	1		
O	0.5379	0.1612	0	1		

space group: *I*4/*m*; tetragonal

Table S3 Rietveld refinement parameters of the M2 sample from Fig. 1b.

Atom	***x***	***y***	***z***	**Occupancy**	***a*(Å)**	***c*(Å)**
H	0.6532	0.5994	0.7281	0.08		
Mn	0.3553	0.1718	0	1	9.789	2.858
O	0.1587	0.1792	0	1		
O	0.5567	0.1477	0	1		

space group: *I*4/*m*; tetragonal

Table S4 Rietveld refinement parameters of the M3 sample from Fig. 1b.

Atom	*x*	*y*	*z*	Occupancy	*a*(Å)	*c*(Å)
H	0.6541	0.5999	0.7827	0.19		
Mn	0.3554	0.1717	0	1		
					9.771	2.856
O	0.1589	0.1782	0	1		
O	0.5401	0.1597	0	1		

space group: *I*4/*m*; tetragonal

Atom	*x*	*y*	*z*	Occupancy	*a*(Å)
Mn	0	0	0	1	
					4.411
O	0.5	0.5	0.5	1	

space group: *Fm*–3*m*; cubic

Table S5 Summary comparison for EWA performances of different absorbers.

Material	Minimum reflection loss (dB)	Thickness (mm) for minimum reflection loss	Effective absorption bandwidth at a thickness
$Ti_3C_2T_x$[5]	−36.3	4.5	4 GHz at 1.5 mm
TiC/MXene nanocomposites[6]	−51.1	3.95	6.08 GHz at 1.55 mm
Nb_2CT_x/α-MnO_2[7]	−24.7	1.8	5 GHz at 1.8 mm
Core-shell δ/α MnO_2[8]	−45.2	3.9	1.5 GHz at 3.9 mm
α-MnO_2[9]	−53.43	4.1	5 GHz at 4.1 mm
α-$Na_{0.05}MnO_2$ nanobelts (M1)	−18.2	3.15	2.9 GHz at 3.15 mm
α-$H_{0.08}MnO_2$ nanobelts (M2)	−22.0	1.4	3.3 GHz at 2 mm

Supplementary References

1 Y. Naito and K. Suetake, *IEEE Trans. Microw. Theory Tech.*, 1971, **19**, 65–72.

2 S. S. Kim, S. B. Jo, K. I. Gueon, K. K. Choi, J. M. Kim and K. S. Churn, *IEEE Trans. Magn.*, 1991, **27**, 5462–5464.

3 M. Cao, X. Wang, W. Cao, X. Fang, B. Wen and J. Yuan, *Small*, 2018, **14**, 1800987.

4 Z. Wu, H. W. Cheng, C. Jin, B. Yang, C. Xu, K. Pei, H. Zhang, Z. Yang and R. Che, *Adv. Mater.*, 2022, **34**, 2107538.

5 B. Fan, N. Li, B. Dai, S. Shang, L. Guan, B. Zhao, X. Wang, Z. Bai and R. Zhang, *Adv. Powder Technol.*, 2020, **31**, 808–815.

6 Y. Chen, F. Wu, S. Zhang, S. Chang, X. Hu, X. Zhang, P. Zhang and H. Zhang, *Compos. Commun.*, 2024, **50**, 102027.

7 X. Wang, C. Yang, Y. Zhang, G. Shi and Y. Zhang, *Mate. Res. Bull.*, 2023, **167**, 112453.

8 T. Su, B. Zhao, B. Fan, H. Li and R. Zhang, *J. Solid. State. Chem.*, 2019, **273**, 192–198.

9 J. Qian, B. Du, C. He, M. Cai, X. Zhong, S. Ren, J. Lou and A. Shui, *J. Am. Ceram. Soc.*, 2022, **105**, 3339–3352.